Dalton Transactions

ROYAL SOCIETY OF CHEMISTRY

PAPER

View Article Online
View Journal | View Issue

Cite this: *Dalton Trans.*, 2024, **53**, 15992

Bioactive Ag(I) coordination complexes as dopants for castor oil plasticized ethylcellulose films†

Francesca Scarpelli, [a] Alessandra Crispini,*[a] Iolinda Aiello, *[a] Nicolas Godbert, [a] Fabio Marchetti, *[b] Sonila Xhafa,[b] Giovanni De Filpo,[c] Mariafrancesca Baratta, [c] Riccardo Berardi,[d] Pasquale Alfano[d] and Eugenia Giorno [a]

The effects exerted by new bioactive acylpyrazolonate Ag(I) derivatives of the general formula **[Ag(Q^{Py,CF3})(R-Im)]** containing different substituents on the imidazole (R-Im) ancillary ligands and the natural plasticizer castor oil when both are added to the ethylcellulose (EC) biopolymer in the preparation of thin films as potential active food packaging materials are presented. The Ag(I) complexes **[Ag(Q^{Py,CF3})(Bn-Im)]** and **[Ag(Q^{Py,CF3})(Bu-Im)]**, having benzyl and butyl substituents, whose single crystal molecular structures are reported, have proved to be highly compatible for efficient incorporation between the EC polymer and the hydrophobic plasticizer chains, giving rise, even at low concentrations, to homogeneous, robust and elastic films. The concomitant presence of these Ag(I) complexes and castor oil in the polymer EC matrix gives rise to thin films with improved antibacterial activity against *Escherichia coli* (*E. coli*) as a model of Gram-negative bacterial strains when compared to the non-plasticized ones, with very low Ag(I) migration in the three food simulants used (distilled water, ethanol 10% v/v and acetic acid 3% v/v) under two assay conditions (70 °C for 2 h and 40 °C for 10 days).

Received 1st August 2024,
Accepted 5th September 2024

DOI: 10.1039/d4dt02201g

rsc.li/dalton

Introduction

The use of plastic materials has become widespread due to their multifunctionality and low cost. This has led to significant plastic waste and a rapid increase in global plastic production, which now exceeds 320 million tons per year.[1] Due to the lack of proper recycling strategies and disposal processes, plastic waste, which hardly breaks down naturally, is mainly released into the environment where it persists and accumulates.[2,3] However, since plastics are lightweight and show noticeable barrier properties, polymers such as polyethylene terephthalate (PET), polyvinyl chloride (PVC), polystyrene (PS) and polypropylene (PP) represent ideal materials for packaging a large variety of food products. On the other hand, while these petroleum-derived materials help reduce the amount of organic waste by increasing food preservation, they also contribute to a significant increase in non-biodegradable plastic waste. To minimize the contamination damage that these plastics cause to the environment, active attempts have been made over the last few years to introduce bio-based materials in food packaging applications.[4,5] Biomaterials, mainly based on natural biopolymers such as starches, cellulose derivatives, chitosan, and pectin, are biodegradable and edible substances.[6,7] Among the most abundant biopolymers in nature, cellulose and its derivatives have emerged as promising materials to be used in food packaging.[8,9] Despite the biodegradability, biocompatibility, low price and high thermal resistance of native cellulose, its strong hydrophilicity, poor solubility, high crystallinity and limited film forming ability drastically limit its use in food packaging applications.[10] On the other hand, ethylcellulose (EC), one of the most significant cellulose derivatives, is a biodegradable, nontoxic and excellent film forming polymer.[11] The ability of EC to incorporate antimicrobial substances and reinforcing agents, together with its hydrophobicity, barrier-forming characteristics, and heat-resistance, makes EC films highly suitable in food packaging applications.[12] Since EC is not in itself an antimicrobial polymer, to achieve active EC packaging films, antimicrobial agents are incorporated within the inner structure of the poly-

[a]*MAT-InLAB, Dipartimento di Chimica e Tecnologie Chimiche, Università della Calabria, 87036 Arcavacata di Rende, CS, Italy. E-mail: a.crispini@unical.it, iolinda.aiello@unical.it*
[b]*School of Science and Technology, Chemistry Section, University of Camerino, Via S. Agostino 1, 62032 Camerino, MC, Italy. E-mail: fabio.marchetti@unicam.it*
[c]*NOPTEA, Dipartimento di Chimica e Tecnologie Chimiche, Università della Calabria, 87036 Arcavacata di Rende, CS, Italy*
[d]*TiFQLab – Centro di sperimentazione ricerca e analisi applicate alle tecnologie alimentari e dell'acqua potabile – Department DIMES, Università della Calabria, 87036 Arcavacata di Rende, CS, Italy*

†Electronic supplementary information (ESI) available. CCDC 2375073 and 2375074. For crystallographic data in CIF or other electronic format see DOI: https://doi.org/10.1039/d4dt02201g

meric matrix during the film forming process. On doing so, EC packaging systems that are able to improve food quality and extend the shelf life can be successfully obtained. Indeed, interesting examples have been reported by using as antimicrobial additives natural molecules such as capsaicin as well as metal nanoparticles with strong antibacterial effects.[13–15] In this regard, bioactive coordination Ag(I) and Cu(II) compounds (BioCCs) and coordination polymers (BioCPs), due to their biological activity and low toxicity to human cells, are nowadays of particular interest in the field of metal-containing additives for multifunctional bioactive polymeric films.[16–19] In particular, silver carrying agents have been and still are the most investigated antimicrobial metal drugs due to their high inhibitory and bactericidal effects.[20,21] Although silver nanoparticles (AgNPs) and Ag salts (AgX) are the most studied forms of antimicrobial additives in polymer matrices, the use of silver coordination compounds and coordination polymers addresses some drawbacks presented by both AgNPs and AgX salts. Since Ag(I) ions are the active component in silver delivery systems, their release in the case of AgNPs depends on several variables, such as nanoparticle size, shape, and surface, often affected by aggregation phenomena compromising their antimicrobial activity,[22] whereas for silver salts the effective release can be limited by the reduction of unshielded Ag(I) ions to metallic silver. Ag(I) complexes and coordination polymers, depending on the choice of coordinated ligands, can overcome these limitations, resulting in more stable species with a slow and consistent release of Ag(I) ions.[23]

On the other hand, the ability of EC to incorporate reinforcing agents such as natural plasticizers represents an additional method not only to obtain EC films for active packaging, but also to improve their mechanical properties, which are partly limited by the semi-crystalline nature of EC.[24,25] Additives such as soybean and sunflower oil can reduce the intermolecular interactions between EC polymer chains, enhancing the free space between polymers and the mobility of chains.[26,27] In this regard, among all vegetable oils, castor oil shows good performance at low temperatures, high kinematic viscosity and excellent lubrication properties.[28–30] The high viscosity of this vegetable oil is rather unusual and is the result of the hydrogen bonding network formed by the hydroxyl group in the predominant ricinoleic fatty acid.[28] It is noteworthy that thin films of EC plasticized with castor oil and containing anthocyanins were recently developed for intelligent packaging to monitor the freshness of pork meat.[31]

In addition, in our research studies on eco-friendly bioactive thin films for food packaging, we recently reported on the preparation and antibacterial properties of EC films embedded with antimicrobial Ag(I) 4-acyl-5-pyrazolonate ($\mathbf{Q^{py}}$) complexes bearing imidazole (**Im**) ancillary ligands.[32] As an extension of our previous work, herein we present the concomitant effects exerted by new Ag(I) derivatives of the general formula **[Ag($\mathbf{Q^{Py,CF3}}$)(R-Im)]** containing different substituents on the **Im** ancillary ligands and the natural plasticizer castor oil when both are added to the EC biopolymer in the preparation of bioactive thin films (Fig. 1).

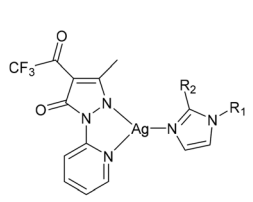

[Ag($\mathbf{Q^{py,CF3}}$)(R-Im)], **1-4**

1, **[Ag($\mathbf{Q^{py,CF3}}$)(Bn-Im)]**, Bn-Im is 1-benzylimidazole, $R_1 = CH_2C_6H_5$; R_2 = H;

2, **[Ag($\mathbf{Q^{py,CF3}}$)(Bu-Im)]**, Bu-Im is 1-butylimidazole, $R_1 = CH_2CH_2CH_2CH_3$; R_2 = H;

3, **[Ag($\mathbf{Q^{py,CF3}}$)(H-Im)]**, H-Im is Imidazole, R_1 = H; R_2 = H;

4, **[Ag($\mathbf{Q^{py,CF3}}$)(Ph-Im)]**, Ph-Im is 2-phenylimidazole, R_1 = H; $R_2 = C_6H_5$;

Fig. 1 Structure of complexes [Ag($\mathbf{Q^{py,CF3}}$)(R-Im)], **1–4**.

All the complexes were synthesised according to the procedure reported in the literature,[33] and the single crystal X-ray structural characterization of complexes **1** and **2** is reported for the first time.

The identification of the best performing **[Ag($\mathbf{Q^{py,CF3}}$)(R-Im)]** complexes with respect to the different substituents held by the **Im** ancillary ligands, their suitable concentration and the right amount of the plasticizer to be used as dopants in the preparation of bioactive EC films has been achieved through both physical-chemical and mechanical characterization. All the new films are tested for their antimicrobial activity against *Escherichia coli* (*E. coli*) as a model of Gram-negative bacterial strains and the results are compared to those obtained from the EC films specifically prepared incorporating only the Ag(I) complexes. Moreover, Ag(I) migration tests towards specific food simulants, according to the EU Food Contact Regulations for Plastics 10/2011 on the migration of chemicals from plastic, are reported.

Experimental

Materials and physical-chemical characterization

All commercial reagents and solvents were purchased from Sigma Aldrich and were used without further purification. The ethylcellulose (EC) used has a degree of substitution equal to 48.0–49.5% (w/w) ethoxyl basis. Castor oil was purchased from AFOM. *E. coli* ATCC 25922 was purchased from Merck.

Infrared (IR) spectra were recorded on a PerkinElmer Spectrum One FT-IR spectrometer. Fourier transform infrared (FT-IR) analysis was carried out on the film samples in the mid-infrared area (4000–400 cm^{-1}) with a PerkinElmer Spectrum 100 FT-IR spectrometer. KBr pellets were prepared only to acquire the spectra of the Ag(I) complexes. Differential Scanning Calorimetry (DSC) analysis was performed using a TA DSC Q2000 instrument with a refrigerated cooling unit (RCS 90). Indium metal standard was used for temperature calibration. The samples were accurately weighed (5–6 mg) and crimped in non-hermetic aluminium pans. The samples were heated at a heating rate of 5 °C min^{-1}, under a dry nitrogen atmosphere (flow rate: 50 ml min^{-1}), using an empty non-hermetic aluminium pan as a reference.

Powder X-ray diffraction (PXRD) measurements were carried out on a Bruker D2-Phaser equipped with Cu Kα radiation

(λ = 1.5418 Å) and a Lynxeye detector, at 30 kV and 10 mA, with a step size of 0.01° (2θ). The obtained diffractograms were analysed using DIFFRAC.EVA diffraction software.

Tensile strength measurements were recorded on a Sauter TVO-S tensile tester equipped with a Sauter FH-1k digital dynamometer and AFH FAST software (Sauter GmbH, Balingen, Germany) at a strain rate of 5 mm min^{-1}. EC-based films were cut into rectangular strips of dimensions 5 cm × 1 cm (length × width).

X-Ray crystallographic analysis

Single crystal X-ray diffraction data of complexes **1** and **2** were collected at room temperature using a Bruker-Nonius X8APEXII CCD area detector system equipped with a graphite monochromator with Mo Kα radiation (λ = 0.71073 Å). In both cases, data were integrated, corrected from absorption effects and scaled using SAINT and SADABS programs.[34–36] Structures were solved by direct methods and refined by full-matrix least squares based on F^2 using the SHELX and SHELXTL software packages.[37,38] All non-hydrogen atoms were refined anisotropically, and hydrogen atoms were included at geometrically calculated positions and refined using a riding model. All graphical representations have been obtained using Olex2-1.5.[39] The details of data collection and structure refinements are reported in the ESI (Table S1†).

Preparation of complexes [Ag($Q^{py,CF3}$)(R-Im)], 1–4

The synthesis procedures of the ligand $HQ^{py,CF3}$ and the Ag(I) complexes **1–3** are reported in literature.[40] On the basis of this synthetic procedure, complex **4** was synthesized for the first time by adding 2-phenyl-imidazole (0.316 g, 2.0 mmol) to a suspension of [Ag($Q^{py,CF3}$)] coordination polymeric species (0.250 g, 0.66 mmol) in acetonitrile (30 mL) solution. A colourless solid was formed slowly and the reaction mixture was stirred at room temperature for 1 h. Subsequently, the solvent was removed using a rotary evaporator and the precipitate was filtered and washed with methanol. The obtained powder was dried *in vacuo*. Yield: 85%. M.p. 140 °C. Anal. calc. for $C_{20}H_{15}AgF_3N_5O_2$: C, 46.00% H, 2.90% N, 13.41% O, 6.13%; found C, 46.38% H, 2.98% N, 13.68%, O, 6.19%; IR (KBr) (ν_{max}/cm^{-1}): 3459m ν, 3060w ν(C atom–H), 1664s ν(C═O), 1592m, 1559m, 1515s, 1434s ν(C═C, C═N, C–N), 1342s, 1302m, 1246s, 953s, 775vs. ^{1}H NMR (DMSO-d6): δH 12.99 (1H, s, –NH), 8.67 (1H, d, J(H–H) = 8.46 H_z, H_d), 8.25 (1H, d, J(H–H) = 4.14 H_z, H_g), 7.99 (2H, d, J(H–H) = 6.9 Hz, H_i), 7.92 (1H, t, J(H–H) = 7.08 Hz, H_f), 7.49–7.41(3H, m, Hi), 7.31 (2H, s, H_h), 7.17 (1H, t, J(H–H) = 4.92 Hz, H_e), 2.29 (3H, s, H_a) ppm.

Preparation of EC-P and EC*nx*-P films (*n* = 1–4, *x* = a–c)

The EC-P films were prepared similarly to the procedure already reported, by adding castor oil to an EC dichloromethane solution.[16,32] In detail, in order to prepare plasticized films with different contents of castor oil (expressed as weight ratios between CO and EC), 1.05 mL (200% w/w, P1), 0.7 mL (134% w/w, P2), 0.3 mL (56% w/w, P3), and 0.15 mL (29% w/w, P4) of the plasticizer were added to 45 mL of a dichloromethane solution containing 0.500 g of EC. In all cases, the solution was thoroughly mixed to help the dissolution process and then poured into a Petri glass dish (9 cm diameter).[32,41,42] The solvent was left to evaporate at room temperature for 24 h and the obtained transparent films were desorbed with 5 mL of distilled water from the glass surface.

All the EC*nx*-P4 films were prepared by adding 0.15 mL of castor oil (29% w/w, P) into 45 mL of a dichloromethane solution containing 0.500 g of EC, followed by the dissolution of different amounts of **[Ag($Q^{py,CF3}$)(R-Im)], 1–4** (2.5%, **a**, 0.05%, **b**, and 0.02%, **c**, weight ratios between the complex and EC). The solutions were stirred for 2 h and then poured into a Petri glass dish (9 cm diameter). After the slow solvent evaporation for 24 h at room temperature, the films were desorbed with 5 mL of distilled water from the glass surface.

The same procedure was used to prepare the reference films without and with castor oil: EC0, EC-$AgNO_3$a–c, EC*nx*, and EC-$AgNO_3$a–c-P4.

Antibacterial activity

The antibacterial activity of all EC films was tested in agreement with the ISO standard. EC films were previously prepared as squares with dimensions of 5 × 5 cm and tested, in triplicate, against *Escherichia coli* (*E. coli*). The EC films were completely immersed in a bacterial aqueous suspension of *E. coli* (112 CFU mL^{-1}, 20 mL) in sterile Petri dishes for 24 h at room temperature. In this way, both faces of the EC films were in contact with the bacterial aqueous suspension. After the contact test, every bacterial aqueous suspension was filtered with a nitrocellulose membrane filter, placed over a plate containing Glucoxane Agar and incubated overnight at 35 ± 1 °C for 24 h. **[Ag($Q^{py,CF3}$)(R-Im)]** unloaded EC-P4 and EC0 samples were used as negative controls, while EC0-P and EC0 loaded with $AgNO_3$ were used as positive controls. In order to evaluate the antibacterial activity of all the silver containing EC films, the % of bacteria growth reduction was calculated by counting the number of bacteria that survived and these values were compared with the number of colonies of the negative control. The percentage of reduction was calculated as previously reported.[32]

Ag(I) migration tests

Inductively Coupled Plasma (ICP) analyses for specific Ag(I) ion migration were carried out using an ICP-OES 5800 VDV optical emission spectrometer. The obtained data were analysed using ICP EXPERT VERSIONE 7.5.3.11953 1.1 FIRMWARE 5395 software. The instrumental limit of quantification (LOQ) of 0.004 mg L^{-1} was determined with the White method and corresponds to that provided by ISO-11885: Waters quality. The determination of selected elements was performed by inductively coupled plasma optical emission spectrometry (ICP-OES).[43]

The Ag(I) migration tests of all the Ag-based films were performed under two different contact conditions and using three different simulants: distilled water (simulant A), ethanol 10% v/v (simulant B) and acetic acid 3% v/v (simulant C). The films, previously cut into squares of dimensions 5 × 5 cm, were

immersed in 50 mL of simulant in a conical flask, so that both faces of the sample were in contact with the simulant. The measurements were performed to correlate Ag(I) migration as a function of contact liquid type, temperature, relative exposure time, and amount of Ag(I) complexes present in the film. All conical flasks, covered with aluminium foil, were kept in a controlled atmosphere under two assay conditions: 40 °C for 10 days and 70 °C for 2 h, according to the EU legislation on the migration of chemicals from plastic materials.[44] Currently, the Food and Drug Administration (FDA/CFSAN) allows the application of silver nitrate ($AgNO_3$) in bottled water and the European Food Safety Authority (EFSA) has declared a specific migration limit of equal to or lower than 0.05 mg kg^{-1} of food.[44,45] After the immersion period, the samples were removed, and the simulant was extracted to analyse the Ag(I) released in the simulants by using ICP-OES. Calibration curves for the investigated element (silver) were obtained by using aqueous standard solutions (3% nitric acid) prepared by appropriate dilution of stock standards. For each sample, three experiments were carried out to evaluate the reproducibility of the release.

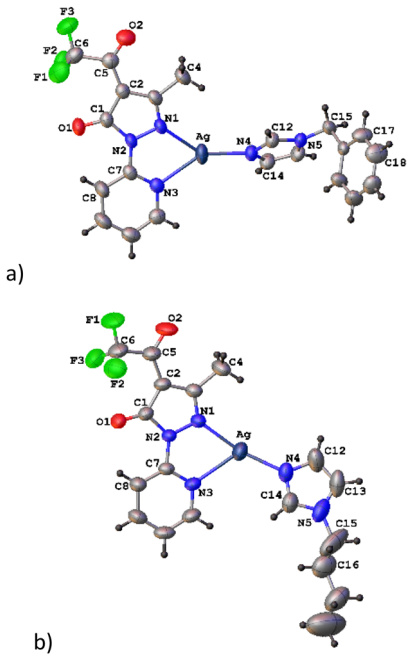

Fig. 2 Molecular structure of (a) **[Ag(Q^{py,CF3})(Bn-Im)]**, **1**, and (b) **[Ag(Q^{py,CF3})(Bu-Im)]**, **2**, with the atomic labelling scheme.

Results and discussion

Ag(I)-based doping agents, [Ag(Q^{py,CF3})(R-Im)], 1–4

The synthesis and complete characterization in solution of the Ag(I) **[Ag(Q^{py,CF3})(R-Im)]** complexes **1–3**, chosen in this work as antimicrobial dopants for the preparation of EC plasticized films to be used as active food packaging materials, as well as their stability as monomeric species, are reported in the literature.[33] Moreover, analogous monomeric Ag(I) species have already been evaluated for their eventual cytotoxic effects when embedded in a polyethylene (PE) matrix, proving to be harmless to human cells. Due to the analogy of complex **4** with derivatives **1–3**, its fundamental characterization has been sufficient to determine the achievement of the expected species. Complexes **1–4** all feature the same N_2-chelated 4-acyl-5-pyrazolonate ligand, but differ in the functionalization at the N4 position of the coordinated imidazole ring. In complexes **1** and **2**, the coordinated **Im** ligand lacks the polar N–H group, with the nitrogen atom bonded to the hydrophobic benzyl and butyl substituents. Differently, complexes **3** and **4**, which both present the N–H functionality, could show a different ability to form intermolecular interactions such as hydrogen bonds both among themselves and with the polymer matrix. Moreover, in complex **4**, the phenyl substituent at the *ortho*-position with respect to the N–H functionality of the coordinated **Im** ligand could exert a steric hindrance, impeding the formation of strong intermolecular interactions. It could be then expected that the different structural features of the four Ag(I) complexes modulate their interactions through their hydrophobic/hydrophilic characteristics with the plasticizer as well as the EC polymer after their incorporation.

Complexes **1** and **2** have been crystallized through slow evaporation of a dichloromethane solution and the single crystal X-ray structural characterization is herein reported. As shown in Fig. 2, the **HQ^{py,CF3}** ligand is found in a monoanionic N_2-chelating mode, with the Ag(I) coordination sphere completed by the imidazole ligand (1-benzylimidazole, Bn-Im, and 1-butylimidazole, Bu-Im) bound through its nitrogen atom.

The bond distances and angles around the Ag(I) ion are comparable to those found in the crystal structure of an analogous Ag(I) complex of the **HQ^{py,CF3}** ligand and similar coordinated imidazole ligands (Table 1).[33] Similarly, a distinct asymmetry between the Ag–N bond distances within the N,N-chelated ring is found, being more pronounced in complex **2** compared to the corresponding values found in the reference compounds. While both complexes show a similar "bite" angle, the trigonal-planar geometry around the metal ion is found to be much more distorted in complex **2** than in **1**. The rotation of the Bn-Im ligand with respect to the N,N-chelated ring in **1** is quite pronounced, with a twist angle around the Ag–N(4) bond of 53.9(3)° and a dihedral angle between its

Table 1 Selected bond distances (Å) and angles (°) of **[Ag(Q^{py,CF3})(Bn-Im)]**, **1**, and **[Ag(Q^{py,CF3})(Bu-Im)]**, **2**

	1	2
Ag–N(1)	2.261(2)	2.195(2)
Ag–N(3)	2.362(2)	2.414(2)
Ag–N(4)	2.141(2)	2.127(3)
N(1)–Ag–N(3)	70.8(1)	71.0(1)
N(1)–Ag–N(4)	143.6(1)	165.3(1)
N(3)–Ag–N(4)	145.1(1)	120.9(1)
N(1)–N(2)–C(7)–N(3)	9.1(3)	1.0(4)

mean plane and the N,N-chelated ring of 48.7(1)°. Moreover, the overall distortion from planarity in **1** is indicated by the torsional angle around the N(2)–C(7) bond within the N,N-chelated ring of 9.1(3)°. The phenyl ring of the imidazole benzyl substituent is nearly perpendicular to the imidazole ring, with a dihedral angle between the two mean planes of 91.3(1)°. The 3D packing of **1** is characterized by weak intermolecular interactions involving the H atoms of the aromatic rings establishing C–H–O and C–H-π contacts with the O atom of the –C═O group of the ligand and the aromatic ring of the imidazole benzyl substituent (Fig. 3a). Moreover, π–π interactions are established between the pyridine ligands of the coordinated acylpyrazolonate ligands. Differently, molecules of complex **2** exhibit a greater tendency towards flatness. In this case, the "twist angle" around the Ag–N(4) bond and the dihedral angle between imidazole and the N,N-chelated ring mean planes have values equal to 7.3(2) and 13.8(1), respectively. The butyl chain bound to the N atom of the imidazole ligand adopts an all-*trans*-configuration in the average molecular plane. In this case, the overall molecular geometry induces the formation of dimers of molecules held together *via* argentophilic interactions, with a minimum Ag–Ag distance of 3.273(1) Å approximately along the *b* direction (Fig. 3b). Within the dimers, weak C–H–F contacts are established with the H atoms of the hydrocarbon chain.

In the *ac* plane, where the average molecular plane lies, one of the imidazole H atoms at the *ortho*-position with respect to the substituted nitrogen atom, is involved in hydrogen bonding (*a* direction) with one of the O atoms of the coordinated $\mathbf{HQ}^{\mathbf{py,CF3}}$ ligand. Moreover, C–H–O and C–H–F contacts are found along the *c* direction (Fig. 3c). The experimental PXRD patterns of complexes **1** and **2** are in agreement with the simulated ones derived from the single X-ray crystal structure (Fig. S1 in the ESI†).

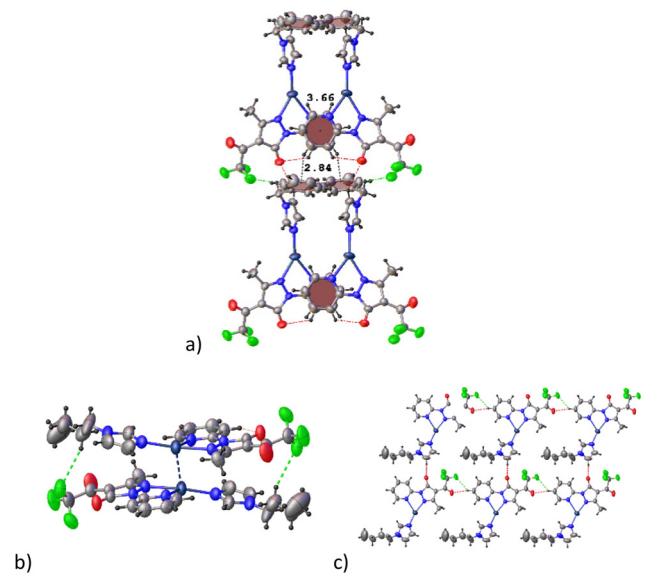

Fig. 3 Crystal packing view of (a) complex **1** (down the *a* direction) showing π–π–π C–H-π, C–H–O and C–H–F interactions, and (b) (c) complex **2** along the *b* direction and in the *ac* plane.

Plasticized EC films

All the EC-based films were prepared by solvent casting, a straightforward method for the preparation of both pristine biopolymeric films and biopolymeric films incorporating active species.[19,46] To determine the suitable amount of castor oil to use as a plasticizer for EC films, different amounts in terms of the weight ratio of the natural plasticizer have been used (see the Experimental section). The occurrence of plasticizers in polymeric matrices can greatly influence their mechanical properties, both in terms of the tensile strength and percentage of elongation at break. Experimental measurements of the EC0 film have shown that it is characterized by a reasonably high Young's modulus (914 ± 42 MPa), indicating robust properties in terms of resistance to deformation before breaking. Nevertheless, its percentage value of elongation at break is extremely poor, only 1.4%, significantly limiting the employment of these eco-friendly materials in food packaging applications. To improve their elastic properties, EC films were doped with different amounts of castor oil (200%, 134%, 56% and 29% w/w, respectively, named EC-P1, EC-P2, EC-P3 and EC-P4), and their mechanical properties were measured and compared to those of the pristine ethylcellulose film (EC0). The results are reported in Table 2, except for EC-P1, whose elevated concentration in castor oil (200% w/w) induced phase separation resulting in a very oily and inhomogeneous film with several cracks, preventing it from being analysed mechanically. Therefore, only EC-P2, EC-P3 and EC-P4 were considered for mechanical investigations. As shown in Table 2, the addition of castor oil leads to a sharp reduction of the Young's modulus of plasticized samples, up to eight times lower than that of pristine EC films. On the other hand, this remarkable decrease in Young's modulus is counterbalanced by a greater elastic character, achieving percentage values of elongation of more than 18% when the lowest amount of castor oil is introduced into the EC polymeric matrix. In consideration of the results reported in Table 2, the sample EC-P4 represents the best compromise between the minimum reduction of Young's modulus and the highest percentage value of elongation when compared to the performances of EC0. Consequently, EC-P1 and EC-P2 were excluded from further investigations with Ag complexes. The stress *vs.* strain plots of EC0, EC-P2, EC-P3 and EC-P4 are reported in Fig. 4.

Table 2 Mechanical properties of EC0, EC-P2, EC-P3 and EC-P4 samples

Sample	Castor oil amount (% w/w)	Young's modulus (MPa)	Elongation at break (%)	Stress (MPa)
EC0	0	914 ± 42	1.4 ± 0.1	12.2 ± 0.9
EC-P2	134	117 ± 7	16.3 ± 0.2	7.7 ± 1.2
EC-P3	56	158 ± 9	15.7 ± 0.2	8.0 ± 1.1
EC-P4	29	180 ± 11	18.6 ± 0.3	8.9 ± 0.8

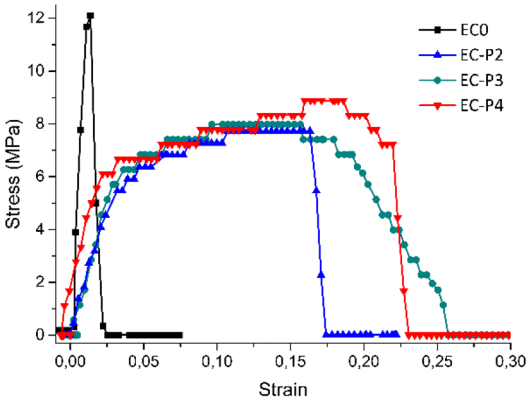

Fig. 4 Comparison of stress *vs.* strain plots between EC films and EC-P films.

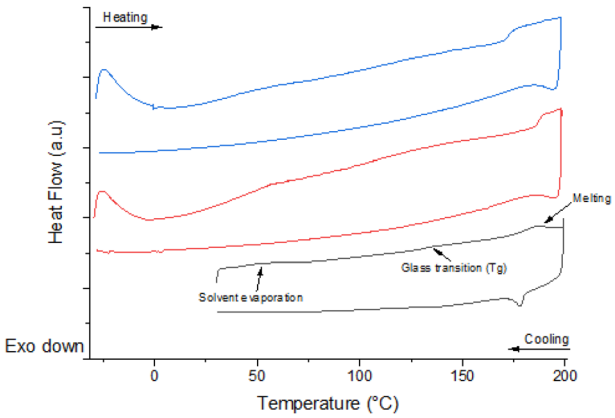

Fig. 5 DSC traces of EC1a-P4 (blue line), EC-P4 (red line) and EC0 (black line) (from ref. 32) obtained at a heating rate of 5 °C min^{-1}.

Upon identifying the EC-P4 film as the best performing one, before the use of the Ag(I) complexes as further dopants into the EC polymeric matrix, its thermal and structural characterization studies have been performed and compared with those of the pure EC film.

As previously reported, the DSC trace of the pure EC polymer presents on heating a first slow endothermal process at low temperature (from 35 °C to 60 °C) characterised by a broad low intensity peak, corresponding to the evaporation of solvent molecules entrapped into the drop-casted film membrane. This process is then followed by a slight change of the slope at *ca.* 135 °C, corresponding to the glass transition temperature (T_g) of the EC polymer, and ultimately by an endothermal process corresponding to the melting of the polymer occurring at *ca.* 183 °C.[32] When castor oil is introduced into the EC0 polymer, even at a low concentration of the plasticizer (29% w/w), the registered DSC trace is characterised by the loss of slope change during heating, thus preventing the exact determination of the glass transition temperature in agreement with an increase of the plasticity of the system. This is accompanied by a broadening of the melting point temperature, which spreads on a wider range of temperatures up to 200 °C. Another piece of evidence of this increase of "fluidity" of the system resides in the absence of the exothermic peak of the crystallization process observed upon cooling. This occurs because castor oil increases the mobility of the polymer chains, thereby enhancing their ability to remain in an amorphous state rather than crystallizing.[47] While for pure EC0, this process occurs upon cooling at *ca.* 178 °C, when castor oil is used, this process is not observed, proving that the presence of the plasticizer impedes the crystallization process (Fig. 5).

To investigate the structural changes of the polymer EC backbone after castor oil incorporation, powder X-ray diffraction (PXRD) analysis was carried out on the plasticized and non-plasticized films. As already reported, the PXRD pattern of EC films casted from dichloromethane solution is characterized by two reflection peaks attributable to the interlayer distance of the ordered polymer structures and to the interchain distance within the same polymer layer, respectively.[32] However, this diffraction profile can also be associated with the lyotropic liquid crystalline nature of EC films, specifically their cholesteric phase. The comparison between EC0 and EC-P4 diffractograms (Fig. 6, black and red lines, respectively) highlights that the two referenced peaks are found at different angle values within the two samples. The first reflection, associated with the interlayer distance and centred at $2\theta = 8.2°$ (d = 10.8 Å) in the EC0 pattern, shifts to a lower angle value, corresponding to a larger d value ($2\theta = 7.2°$; d = 12.2 Å), in the diffraction profile of EC-P4.[32]

This finding, already reported for other plasticized polymers, clearly demonstrates the effectiveness of the plasticizer in intercalating between the layers of the polymer chains, reducing the intermolecular interactions existing between them.[48–50] Moreover, in the EC0-P pattern, the second peak, arising from the interchain distance within the same polymer layer, shifts to slightly higher angles (2θ = 20.2°), corresponding to smaller d-spacings (d = 4.4 Å), compared to the EC0 pattern ($2\theta = 19.2°$; d = 4.6 Å). This may also be ascribed to the interposition of the plasticizer between the polymer

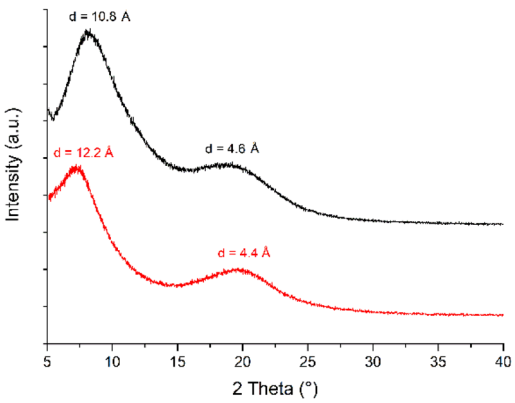

Fig. 6 PXRD patterns of EC0 (black line) and EC-P4 (red line).

layers, which forces the chains within each layer to pack more closely.

Ag(I)-based plasticized films (EC*nx*-P, *n* = 1–4, *x* = a–c)

The Ag(I)-doped films were formulated at three different concentrations of the Ag(I) species (2.5%, 0.05%, and 0.02% w/w, with respect to EC). The most concentrated films (2.5% w/w) were prepared and used exclusively for the physico-chemical characterization of these materials. In fact, any structural changes in the polymer matrix resulting from the interaction of EC and eventually castor oil with the Ag(I) complexes would not be detectable in more diluted samples. The significantly reduced concentrations of 0.05% and 0.02% w/w were chosen to verify the antimicrobial activity of the derived films even in the presence of a low amount of silver derivatives.

The introduction of Ag(I) complexes into plasticized films can alter the internal polymer structure by the establishment of new chemical interactions between the EC polymer chains, plasticizer and Ag(I) derivatives. Therefore, the mechanical properties of the plasticized films doped with Ag(I) were properly investigated in order to find which Ag(I) complex, and in what percentage, can ensure a mechanical behaviour of the derived film similar to or even better than that of EC-P4. Since EC0 is poorly elastic and highly stiff, the mechanical characterization of the non-plasticized EC films containing the Ag(I) complexes was not performed. Furthermore, since $AgNO_3$ is the standard reference material in antibacterial tests, EC-P4 films containing $AgNO_3$ in different weight amounts were also prepared and their mechanical properties were evaluated on par with the other samples. All experimental results are reported in Fig. 7 and Table S2.†

What immediately stands out is that Ag(I) doping enhances film robustness, with Young's modulus values higher than that of EC-P4 (180 MPa) and quite similar to that of the pristine EC0 film (914 MPa) (Fig. 7). Nonetheless, the elastic properties are clearly reduced, going back to very poor values, especially when complexes **3** and **4** are used as dopant agents (Fig. 7). In contrast, interesting results are obtained with complex **2**, where the film at 0.05% w/w concentration exhibits a Young's modulus of 418 MPa, two times higher than that of EC-P4, and a percentage of elongation of 21%, representing an additional 13% increase over the corresponding value in EC-P4. This improvement in both directions, robustness and elasticity, proves that complex **2** manages to insert itself into the hydrocarbon chains of both castor oil and the EC polymer *via* compatible intermolecular interactions with the substituent on the imidazole ring, without altering in a substantial way the structure of the neat EC-P4 film.

When the Ag(I) complexes are blended together with castor oil into the polymer EC matrix, the only observable change is the decrease of the melting point temperature of the polymer by a few degrees, while the DSC thermogram is still characterised by a relative broadening of the melting point endothermic peak that spreads from 177 °C up to *ca.* 200 °C. Fig. 5 reports the DSC trace of the EC1a-P4 film as an example, together with the traces of the EC-P4 blend and pure EC0 for a direct comparison. A similar behaviour is observed for all complexes (Fig. S2 in the ESI†).

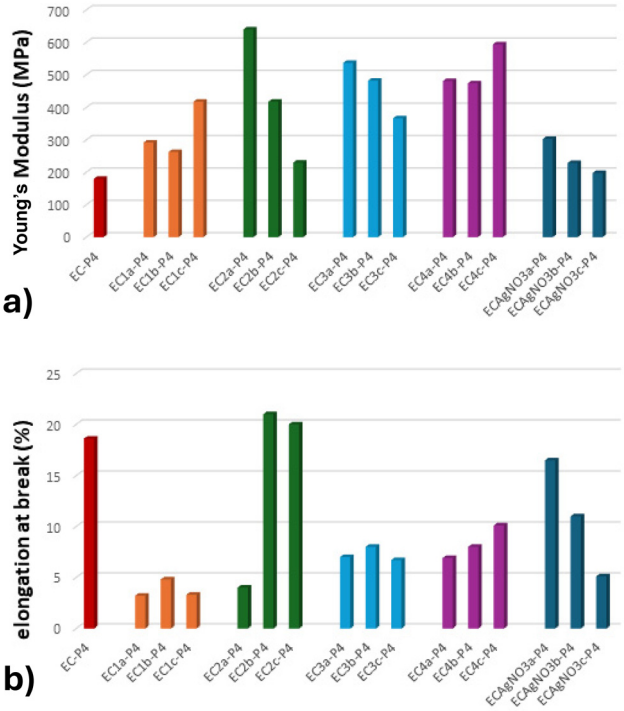

Fig. 7 Young's modulus (a) and elongation at break (b) for the tested samples.

The PXRD patterns of the plasticized films containing the Ag(I) complexes, compared to the corresponding non-plasticized samples and to the reference matrices EC0 and EC0-P, are illustrated in Fig. 8. The effectiveness of the plasticizer persists even in the presence of Ag(I) complexes within the

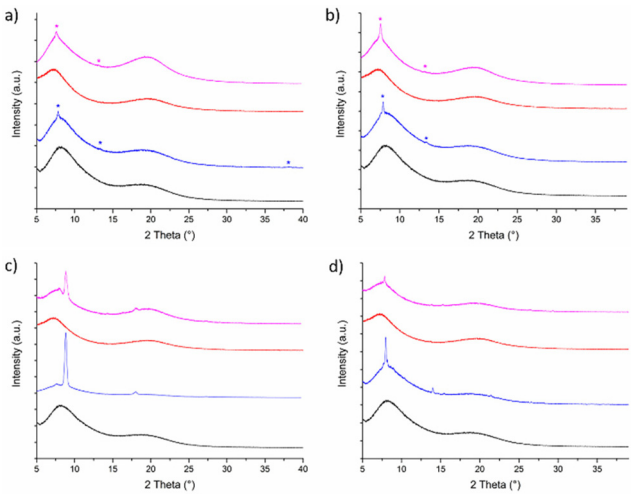

Fig. 8 PXRD patterns of (a) EC0, EC1a, EC-P4 and EC1a-P4; (b) EC0, EC2a, EC-P4 and EC2a-P4; (c) EC0, EC3a, EC-P4 and EC3a-P4; and (d) EC0, EC4a, EC-P4 and EC4a-P4. In all patterns: EC-P4 and EC0: red and black lines and EC*n*a-P4 and EC*n*a: pink and blue lines.

polymer matrix, since the PXRD patterns of all the Ag(I)-containing plasticized films (Fig. 8, pink lines) exhibit reflections associated with the interlayer and interchain distances at the same positions as in the EC0-P4 film (Fig. 8, red lines), thus shifted with respect to the corresponding non-plasticized films (Fig. 8, blue lines). Previously, it has been demonstrated that complex **1** displays a strong affinity toward the EC polymer matrix.[32] In fact, upon the incorporation of complex **1** into the EC polymer matrix, a local hexagonal sub-organization of the polymer backbone, which coexists with the chiral nematic order (N*), is formed. This is evidenced by the emergence of three weak reflections in the typical diffraction profile of EC0, as seen in the PXRD pattern of EC1a (Fig. 8a, blue line, reflections are marked with stars). These diffraction peaks correspond to interplanar spacings of d = 11.26 Å, 6.6 Å, and 2.4 Å, and can be indexed to a 2D hexagonal lattice (H). The same applies when complex **1** is incorporated into EC0 in the presence of castor oil (Fig. 8a, pink line), with weak reflections, consistent with a 2D hexagonal lattice, occurring at the same d-values as in the corresponding non-plasticized film. A similar phenomenon is observed when complex **2** is incorporated into the polymer, as the diffraction peaks, associated with the hexagonal sub-organization of the EC matrix, also appear in the PXRD patterns of EC2a and EC2a-P4 (Fig. 8b, blue and pink lines, respectively; reflections are marked with stars). The explanation for this observation lies in the similar structures of the two complexes, which allow for efficient incorporation between the polymer chains, thus modifying the organization of the polymer matrix. Moreover, the presence of castor oil, hydrophobic in nature, does not change the miscibility of both complexes **1** and **2** with the ethylcellulose polymer; in contrast, it forms a perfectly homogeneous blend.

A different situation is observed when complexes **3** and **4** are incorporated into the polymer matrix, both in the presence and absence of the plasticizer. Indeed, in the diffraction profiles of EC3a, EC3a-P4, EC4a and EC4a-P4 (Fig. 8c and d, blue and pink lines), the distinctive reflections of these Ag(I) compounds (Fig. S3c and S3d in the ESI†) arise from the typical diffraction profile of EC. This finding clearly indicates that the crystallization of complexes **3** and **4** occurs during the film forming process in both plasticized and non-plasticized cases, leading to the formation of inhomogeneous samples. Finally, the PXRD patterns of the films containing $AgNO_3$, EC$AgNO_3$a and EC$AgNO_3$a-P4, are perfectly superimposable with the corresponding PXRD patterns of the reference films, EC0 and EC-P4, respectively (Fig. S4 in the ESI†). The absence of both characteristic $AgNO_3$ reflections and new diffraction peaks, as previously observed in plasticizer-free EC films, indicates excellent incorporation of the salt into the polymer matrix, effectively acting as a solvent-like dispersive medium for $AgNO_3$.

The FT-IR spectra of the Ag(I)-incorporating films, along with those of the corresponding Ag(I) complexes, are illustrated in Fig. 10, and compared to those of EC0 and EC0-P (Fig. 9). First of all, the addition of castor oil to the EC polymer is evident due to the presence of the 1743 cm^{-1} band in the spectrum of EC0-P (Fig. 9, red line; the band is marked with a triangle), which is characteristic of the C=O vibration of the ester groups of the plasticizer.

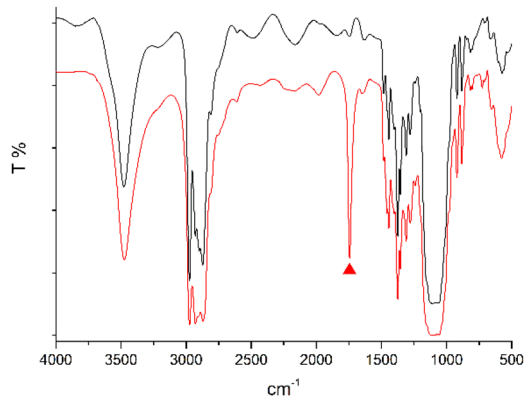

Fig. 9 FT-IR spectra of EC0 (black line) and EC-P4 (red line).

With the addition of the Ag(I) complexes, the ester band remains unchanged, indicating the absence of significant interactions between the plasticizer and the Ag(I) compounds (Fig. 10). In addition, the FT-IR spectra of the Ag(I)-containing films, both plasticized and non-plasticized (Fig. 10, pink and blue lines, respectively), show no significant differences compared to the undoped films. However, some differences are observed between the spectra of the Ag(I)-containing films and those of the corresponding Ag(I) complexes. Specifically, the band at *ca.* 1665 cm^{-1}, arising from the C=O stretching vibrations of the Ag(I) complex carbonyl groups, shifts to a higher wavenumber in the spectra of the corresponding films (Fig. 10). As previously reported, this finding suggests the existence of weak van der Waals interactions between the polymer and the Ag(I) additives.[32,51] However, this effect is negligible in the film containing complex **3**, while it is enhanced in the

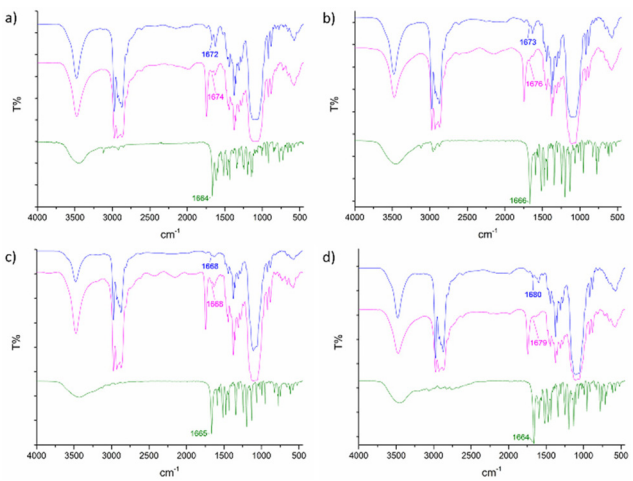

Fig. 10 FT-IR spectra of (a) EC1a, EC1a-P4 and complex **1**; (b) EC2a, EC2a-P4 and complex **2**; (c) EC3a, EC3a-P4 and complex **3**; and (d) EC4a, EC4a-P4 and complex **4**. Non-plasticized and plasticized films: blue and pink lines and complexes **1–4**: green line.

FT-IR spectra of the films incorporating the other Ag(I)-compounds. This indicates that the presence of benzyl, butyl, and phenyl substituents on the imidazole ring of complexes **1**, **2** and **4**, respectively, plays a significant role in the interaction with the matrix.

Antibacterial activity

Food-borne diseases caused by microorganisms (bacteria, viruses, fungi, and other parasites) are at the origin of a significant number of human illnesses.[52] The most common bacterial pathogens are pathogenic *Escherichia coli* (*E. coli*), *Salmonella* spp., *Campylobacter* spp., *Staphylococcus aureus, Clostridium perfringens*, *Listeria monocytogenes*, *Shigella* spp., and *Cronobacter sakazakii*.[53] In this work, as preliminary studies of the antibacterial activity of all new plasticized EC*nx*-P4 films, *Escherichia coli* has been chosen as a model of Gram-negative bacterial strains, in comparison with our previous studies conducted on non-plasticized EC films containing similar Ag(I) additives.[32] EC-P4, EC0, ECAgNO$_3$-P4 and ECAgNO$_3$, at various concentrations, were tested as negative and positive controls, respectively. The results of the antibacterial activities shown by EC*nx*-P4 and EC*nx* films, expressed as the relative killing percentage (%), according to the ISO standard, are reported in Tables S3 and S4 in the ESI.† The obtained data are shown in Fig. 11 only for the films, both plasticized and non-plasticized, containing a minor amount of **[Ag(Q^{py,CF3})(R-Im)]** complexes, **1–4**.

The embedding of silver derivatives introduces antibacterial activity even at low concentrations in all cases. However, only in the EC1b,c-P4, EC2b,c-P4 and EC3c-P4 films, the concomitant presence of the plasticizer and the Ag(I) additives in the EC polymer makes the derived films more active against *E. coli* with respect to the non-plasticized ones. The best relative killing percentage is found in the case of EC1b-P4 and EC2b-P4 films, containing complexes **[Ag(Q^{py,CF3})(Bn-Im)]**, **1**, and **[Ag(Q^{py,CF3})(Bu-Im)]**, **2**, in a concentration of 0.05% w/w, whose activities are comparable with that found for ECAgNO$_3$b-P4. These results are particularly encouraging since in the Ag(I) complexes under study, the concomitant presence of the coordinated 4-acyl-5-pyrazolone and the imidazole ligands, both biologically active organic molecules,[54] synergistically imparts a significant bactericide behavior at least against *E. coli* even in the absence of water solubility.

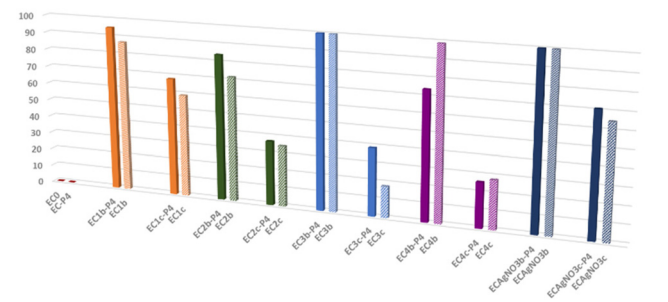

Fig. 11 Antibacterial activity, expressed as the relative killing percentage (%) of EC*n*b,c-P4 and EC*n*b,c films and relative controls.

Release tests of Ag(I) migration

Ag(I) migration from the new EC*nx*-P4 films has been tested by using three food simulants, corresponding to a different food class, depending on the pH. In particular, distilled water (A), ethanol 10% v/v (B) and acetic acid 3% v/v (C) have been chosen and all were used under two assay conditions, 70 °C for 2 h and 40 °C for 10 days, according to the EU legislation on the migration of chemicals from plastic materials.[44] The measurements have been performed in order to correlate Ag(I) migration as a function of contact liquid type, temperature and relative exposure time, in relation to the amount of Ag(I) complexes introduced together with the plasticizer into the EC matrix. Presently, the Food and Drug Administration (FDA/CFSAN) allows the application of $AgNO_3$ in bottled water and the European Food Safety Authority (EFSA) has declared a specific migration limit of equal to or lower than 0.05 mg kg^{-1} of food.[44,45] ECP4 and EC-AgNO$_3$a–c-P4 were tested respectively as negative and positive controls, with the ECP4 film showing a total absence of Ag(I) ions and assuming the maximum migration of free Ag(I) ions from EC-AgNO$_3$a–c-P4 films. To understand the role of castor oil in combination with the Ag(I) derivatives, identical measurements were performed on non-plasticized EC*nx* films as well as on their negative and positive EC0 and EC-AgNO$_3$a–c controls. The Ag(I) migration values expressed in terms of milligrams per volume at the different concentrations and under different working conditions are reported in Tables S5–S8 (ESI†), while in Fig. 12–17 only the data of the films, both plasticized and non-plasticized, containing a minor amount of **[Ag(Q^{py,CF3})(R-Im)]** complexes, **1–4**, are presented.

As shown in Fig. 12–17, the addition of complexes **1** and **2** and castor oil into the EC polymer matrix produces a distinct effect of Ag(I) release with respect to complexes **3** and **4**, despite the simulant and the assay conditions. Indeed, in the case of EC1b,c-P4 and EC2b,c-P4, the Ag(I) migration values are always below the limit set by the EU legislation of

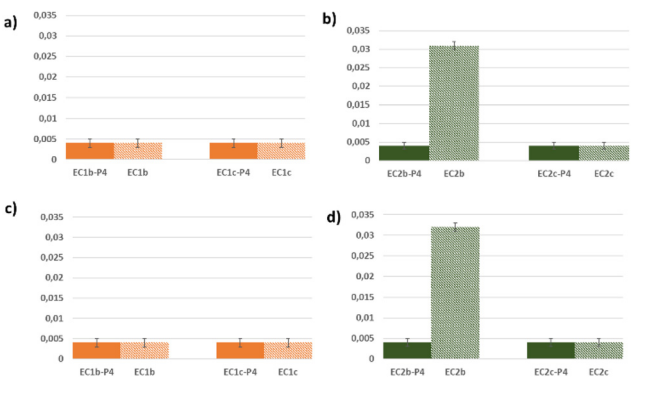

Fig. 12 Ag(I) migration values in milligrams per volume of EC1b,c-P4, EC1b,c, EC2b,c-P4 and EC2b,c films in simulant A at (a) and (b) 2 h and 70 °C and (c) and (d) 10 days at 40 °C.

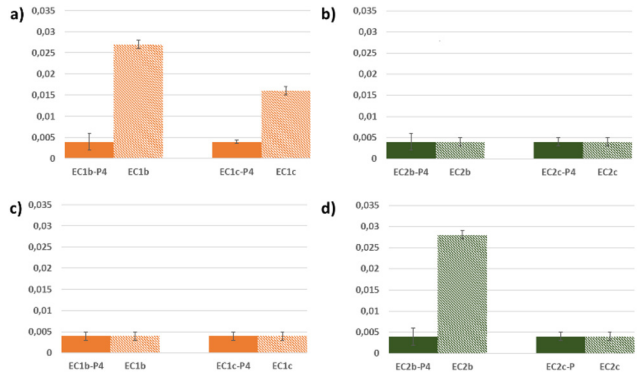

Fig. 13 Ag(I) migration values in milligrams per volume of EC1b,c-P4, EC1b,c, EC2b,c-P4 and EC2b,c films in simulant B at (a) and (b) 2 h and 70 °C and (c) and (d) 10 days at 40 °C.

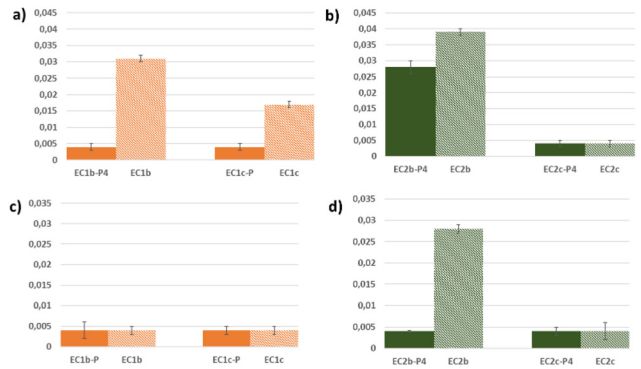

Fig. 14 Ag(I) migration values in milligrams per volume of EC1b,c-P4, EC1b,c, EC2b,c-P4 and EC2b,c films in simulant C at (a) and (b) 2 h and 70 °C and (c) and (d) 10 days at 40 °C.

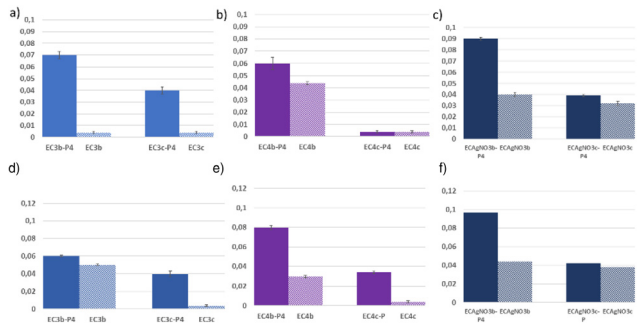

Fig. 15 Ag(I) migration values in milligrams per volume of EC3b,c-P4, EC3b,c, EC4b,c-P4, EC4b,c, ECAgNO3b,c-P4 and ECAgNO3b,c films in simulant A at (a), (b) and (c) 2 h and 70 °C and (d), (e) and (f) 10 days at 40 °C.

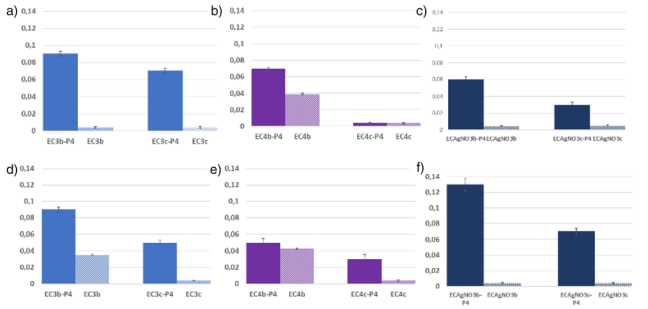

Fig. 16 Ag(I) migration values in milligrams per volume of EC3b,c-P4, EC3b,c, EC4b,c-P4, EC4b,c, ECAgNO3b,c-P4 and ECAgNO3b,c films in simulant B at (a), (b) and (c) 2 h and 70 °C and (d), (e) and (f) 10 days at 40 °C.

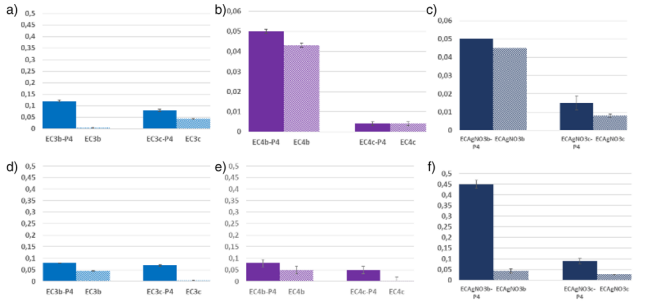

Fig. 17 Ag(I) migration values in milligrams per volume of EC3b,c-P4, EC3b,c, EC4b,c-P4, EC4b,c, ECAgNO3b,c-P4 and ECAgNO3b,c films in simulant C at (a), (b) and (c) 2 h and 70 °C and (d), (e) and (f) 10 days at 40 °C.

0.05 mg kg^{-1} or the instrumental limit of quantification (LOQ) of 0.004 mg L^{-1}, and equal to or lower than the corresponding values found for the non-plasticized EC1b,c and EC2b,c (Fig. 12, 13 and 14) films.[43] Another important common aspect is that in EC1b,c-P4 and EC2b,c-P4, the Ag(I) migration is not concentration dependent, with the only exception being EC2b-P4 in simulant C at the shortest exposure time and at the highest temperature (Fig. 14b).

In distilled water (simulant A), the effect of the presence of the plasticizer is much more evident in the presence of complex **2**, where the difference in Ag(I) migration is very significant with respect to the non-plasticized film at the 0.05% weight ratio between the complex and EC under both working conditions (Fig. 12b and d). Differently, in simulants B and C, the greatest difference between the plasticized and non-plasticized EC films is clearly dependent on the working conditions (Fig. 13 and 14). Indeed, in simulant B, the reduction of the swelling effect exerted by ethanol on the EC polymeric matrix[55] in the plasticized films is favoured by a temperature of 70 °C and an exposure time of 2 h in the case of EC1b-P4, while for EC2b-P4, a lower temperature and a longer exposure time are necessary (Fig. 13a and d). Even if both complexes **1** and **2** show structures compatible with efficient incorporation between the EC polymer chains and the hydrophobic plasticizer, thereby forming perfectly homogeneous blends, some differences in Ag(I) migration in the various simulants and under the different working conditions can only be revealed at a higher content of complexes within the films. As reported in Tables S3 and S4,† the Ag(I) migration from EC2a-P4 films is generally lower than that observed in the case of the EC1a-P4

ones, at 70 °C and two hours of exposure and in the three simulants, while the opposite trend is recorded when lowering the temperature and increasing the time of exposure. The presence of the butyl substituent on the **Bu-Im** ligand in complex **2** yields a predominance of hydrophobic interactions with the aliphatic chains of the environment (both castor oil and EC polymer) compared to what can be hypothesized in the case of complex **1**. Indeed, in **1**, the presence of the phenyl ring in the coordinated **Bn-Im** ligand introduces more interactions such as aromatic ones, as already highlighted by the analysis of the intermolecular interactions in the solid crystalline state. Therefore, as an attempt of explanation, at high temperature, the increased motion induced on the rotationally free phenyl ring of the **Bn-Im** coordinated ligand in complex **1** causes the weakening of the aromatic interactions established within the polymeric matrix, with the consequent increase of silver migration. This effect is particularly evident in simulants B and C. While in simulant B, a concomitant swelling effect of the polymer EC matrix in the presence of ethanol amplifies the effect of Ag(I) release, in simulant C, degradation effects in an acidic medium may not be irrelevant (Table S4 in the ESI†). On the other hand, at a lower temperature and a longer exposure time, an opposite trend in silver migration between EC1a-P4 and EC2a-P4 is observed (Table S5 in the ESI†).

The cooperative hydrophobic and aromatic intermolecular interactions between complex **1** and the plasticized EC polymer matrix help keep the complex molecules tightly embedded within the system for a longer time, with a consequent reduction of silver migration with respect to EC2a-P4 films.

In all cases, the Ag(I) migration from EC1b,c-P4 and EC2b,c-P4 films is always found to be lower than that recorded for the reference EC-AgNO3b,c-P4 films (Fig. 15–17). Indeed, when $AgNO_3$ is embedded with castor oil within the EC matrix, the Ag(I) release from the resulting films is concentration dependent, higher than that from the non-plasticized ones and, in the case of 0.05% w/w concentration, it is higher than the limit set by the EU legislation (0.05 mg kg^{-1}). As proved by the PXRD pattern of the $AgNO_3$a-P4 film (Fig. S3 in the ESI†), even in the presence of the plasticizer, the Ag(I) salt is deeply and homogeneously dispersed within the matrix, similar to the case of the non-plasticized film.[32] Even if Ag(I) ions do not cause any inner or surface structural variation of the polymeric backbone, the presence of castor oil, inducing a kind of inner "fluidity", favors a greater mobility of the free ions, increasing their release when compared to the non-plasticized films.

The same trends in terms of Ag(I) release are observed in the case of EC3b,c-P4 and EC4b,c-P4 films when compared to the non-plasticized ones (Fig. 15–17). In these cases, both complexes give rise to inhomogeneous films, crystallizing on their surface (see PXRD characterization), regardless of the presence or absence of the plasticizer. However, the major Ag(I) release from EC3b,c-P4 and EC4b,c-P4 films when compared to the non-plasticized ones could be explained by the significant incompatibility between both complexes and the hydrophobic plasticizer.

Generally, the highest values of Ag(I) migration are detected in all simulants A, B and C under both working conditions, at a complex concentration of 0.05% w/w, overcoming the limit set by the EU legislation of 0.05 mg kg^{-1}. The Ag(I) release decreases on decreasing the amount of complexes **3** and **4** added to the EC matrix. No significant difference is observed in the Ag(I) migration values between the EC3-P4 and EC4-P4 films in all the complex concentrations, in all simulants and under the working conditions used in Fig. 15–17 and Tables S6 and S7 in the ESI.†

Conclusions

[Ag($Q^{py,CF3}$)(R-Im)] complexes, **1–4**, have been used in this work as bioactive dopants for the preparation of EC films in conjunction with the natural plasticizer castor oil as potential active food packaging materials. Upon identifying the best concentration of castor oil to be used to obtain films with better mechanical properties compared to the pristine EC polymer, the effects of different substituents on the N atom of the coordinated **Im** ligands in the Ag(I) complexes have been determined. Indeed, the nature of the substituents has been shown to play a key role in the formation of highly homogeneous, robust and elastic films. Both complexes **1** and **2**, showing benzyl and butyl substituents respectively, have proved to have structures compatible with efficient incorporation between the EC polymer and the hydrophobic plasticizer chains, when compared to complexes **3** and **4**. In the latter cases, the presence of the N–H functionality on the coordinated **Im** ligand yields the strong tendency of complexes **3** and **4** to crystalize during the film forming process, leading to the formation of inhomogeneous samples. All EC1*x*-P4 and EC2*x*-P4 films (*x* is the content of the Ag(I) complex within the plasticized EC polymer) have shown better mechanical properties with respect to the non-plasticized films, particularly relevant in the case of the use of the **[Ag($Q^{py,CF3}$)(Bu-Im)]** complex, **2**, at 0.05% w/w concentration. The best robustness and elasticity found for the EC2b-P4 film prove the ability of molecules of **2**, more than that of complex **1**, to match very well with the hydrocarbon chains of both castor oil and the EC polymer, becoming part of the entire blend. To this end, as shown by the crystal structure determination of **1** and **2**, the presence of the butyl chain instead of the bulky benzyl substituent on the imidazole ligand endows molecules of **2** with a greater tendency towards flatness, increasing their ability to interpenetrate between the castor oil and EC polymer chains. The addition of the Ag(I) derivatives introduces antibacterial activity against *E. coli* even at low concentrations. Moreover, the concomitant presence in the EC polymer of the plasticizer and the Ag(I) additives makes the derived films more active with respect to the non-plasticized ones. Particularly relevant is the case of EC1b-P4 and EC2b-P4 films, containing complexes **[Ag($Q^{py,CF3}$)(Bn-Im)]**, **1**, and **[Ag($Q^{py,CF3}$)(Bu-Im)]**, **2**, in a concentration of 0.05% w/w, whose activities are comparable with that found for EC$AgNO_3$b-P4. Measurements of Ag(I) migration in three food simulants, distilled water (A), ethanol 10% v/v (B) and acetic acid 3% v/v (C), and under two assay

conditions, 70 °C for 2 h and 40 °C for 10 days, have been performed to verify the ability of the EC plasticized matrix to deeply incorporate the Ag(I) antimicrobial dopants. Only in the case of EC1*x*-P4 and EC2*x*-P4 films with lower contents of Ag(I) complexes (x = 0.05 and 0.02 w/w), Ag(I) migration is not concentration dependent, lower than that observed in the non-plasticized films and lower than the limit set by the EU legislation (0.05 mg kg^{-1}), regardless of the working conditions. On the other hand, the higher Ag(I) release from EC3b,c-P4 and EC4b,c-P4 films than from the non-plasticized ones could be a sign of the intimate incompatibility between both complexes and the hydrophobic plasticizer.

Author contributions

F. S.: conceptualization and investigation; A. C.: conceptualization, supervision, and writing – original draft; I. A.: validation and writing – review & editing; N. G.: investigation; F. M.: investigation and validation; S. X.: investigation; G. D. F. & M. B.: investigation; R. B. & P. A.: resources; E. G.: investigation and validation.

Data availability

The data supporting this article have been included as part of the ESI.†

Crystallographic data for **1** and **2** have been deposited at the CCDC under 2375073 and 2375074.†

Conflicts of interest

There are no conflicts to declare.

Acknowledgements

The present work was partially financed by "Progetto STAR 2 (PIR01_00008)" – Italian Ministry of University and Research. A. C. is grateful to the project PRIN 2022 PNRR "P2022TMJ8T – Combining natural polymer-based hydrogel/aerogel with highly porous materials for selective CO2 capture from gaseous stream" (CUP:H53D23008010001).

F. S. is grateful to the project PON "Ricerca e Innovazione" 2014–2020, Asse IV "Istruzione e ricerca per il recupero" and Azione IV.6 "Contratti di ricerca su tematiche Green" (CUP: H25F21001230004; identification code: 1062_R8_GREEN).

The University of Camerino is gratefully acknowledged for having financed part of S. X.'s doctoral scholarship. This work was also financially supported by MUR – PNRR (Decreto Direttoriale n. 703 del 20-4-2022), within the framework of the project "VITALITY – Innovation, digitalisation and sustainability for the diffused economy in Central Italy" (cod. ECS_00000041), Spoke 9 – Nanostructured materials and devices.

References

1 S. L. Wright and F. J. Kelly, *Environ. Sci. Technol.*, 2017, **51**, 6634–6647.
2 P. Pandey, M. Dhiman, A. Kansal and S. P. Subudhi, *Waste Dispos. Sustain. Energy*, 2023, **5**, 205–222.
3 A. Tursi, M. Baratta, T. Easton, E. Chatzisymeon, F. Chidichimo, M. De Biase and G. De Filpo, *RSC Adv.*, 2022, **12**, 28318–28340.
4 M. E. González-López, S. de J. Calva-Estrada, M. S. Gradilla-Hernández and P. Barajas-Álvarez, *Front. Sustain. Food. Syst.*, 2023, **7**, 1225371.
5 Y. A. Shah, S. Bhatia, A. Al-Harrasi and T. S. Khan, *Biotechnol. Sustain. Mater.*, 2024, **1**, 2.
6 K. Y. Perera, A. K. Jaiswal and S. Jaiswal, *Foods*, 2023, **12**, 2422.
7 J. Cheng, R. Gao, Y. Zhu and Q. Lin, *Alexandria Eng. J.*, 2024, **91**, 70–83.
8 S. Romão, A. Bettencourt and I. A. C. Ribeiro, *Polymers*, 2022, **14**, 4968.
9 A. Irimia, V. C. Grigoraș and C.-M. Popescu, *Polymers*, 2024, **16**, 389.
10 X. Liu, Z. Qin, Y. Ma, H. Liu and X. Wang, *J. Renewable Mater.*, 2023, **11**, 3203–3225.
11 P. Ahmadi, A. Jahanban-Esfahlan, A. Ahmadi, M. Tabibiazar and M. Mohammadifar, *Food Rev. Int.*, 2022, **38**, 685–732.
12 Y. Liu, S. Ahmed, D. E. Sameen, Y. Wang, R. Lu, J. Dai, S. Li and W. Qin, *Trends Food Sci. Technol.*, 2021, **112**, 532–546.
13 A. Balciunaitiene, V. Januskevice, S. Saunoriute, U. Raubyte, J. Viskelis, P. B. Memvanga and P. Viskelis, *Polymers*, 2024, **16**, 317.
14 X. Su, Z. Yang, K. B. Tan, J. Chen, J. Huang and Q. Li, *Carbohydr. Polym.*, 2020, **241**, 116259.
15 V. Chandrababu, J. Parameswaranpillai, J. A. Gopi, C. Pathak, C. D. Midhun Dominic, N. L. Feng, S. Krishnasamy, C. Muthukumar, N. Hameed and S. Ganguly, *Biomater. Adv.*, 2024, **162**, 213921.
16 A. Crispini, I. Aiello, N. Godbert, M. La Deda, G. Di Maio, A. Tagarelli, R. Elliani, R. De Rose and F. Scarpelli, *Chem. – Eur. J.*, 2024, **30**, e202400452.
17 T. A. Fernandes, F. Macedo, R. G. Cabral, T. Guiu, C. H. J. Franco, P. Jorge, A. C. Sousa, V. André, N. Cerca and A. M. Kirillov, *RSC Appl. Interfaces*, 2024, **1**, 98–109.
18 T. A. Fernandes, I. F. M. Costa, P. Jorge, A. C. Sousa, V. André, N. Cerca and A. M. Kirillov, *ACS Appl. Mater. Interfaces*, 2021, **13**, 12836–12844.
19 K. I. Trusau, P. Jorge, A. C. Sousa, T. A. Fernandes, V. André, M. V. Kirillova, A. I. Usevich, N. Cerca and A. M. Kirillov, *RSC Sustainability*, 2023, **1**, 866–875.
20 A. Frei, A. D. Verderosa, A. G. Elliott, J. Zuegg and M. A. T. Blaskovich, *Nat. Rev. Chem.*, 2023, **7**, 202–224.
21 A. Crispini, M. La Deda, G. Di Maio, N. Godbert, A. Tagarelli, R. Elliani, A. Candreva, R. De Rose, I. Aiello, M. Amati and F. Scarpelli, *Cryst. Growth Des.*, 2023, **23**, 3518–3534.

22 P. Bélteky, A. Rónavári, D. Zakupszky, E. Boka, N. Igaz, B. Szerencsés, I. Pfeiffer, C. Vágvölgyi, M. Kiricsi and Z. Kónya, *Int. J. Nanomed.*, 2021, **16**, 3021–3040.
23 L. Ronga, M. Varcamonti and D. Tesauro, *Molecules*, 2023, **28**, 4435.
24 A. Narayanan, M. Friuli, A. Sannino, C. Demitri and L. Lamanna, *Carbohydr. Polym. Technol. Appl.*, 2023, **6**, 100378.
25 D. Yang, X. Peng, L. Zhong, X. Cao, W. Chen, X. Zhang, S. Liu and R. Sun, *Carbohydr. Polym.*, 2014, **103**, 198–206.
26 M. E. Aulton, M. H. Abdul-Razzak and J. E. Hogan, *Drug Dev. Ind. Pharm.*, 1981, **7**, 649–668.
27 B. D. Rohera and N. H. Parikh, *Pharm. Dev. Technol.*, 2002, **7**, 421–432.
28 D. Ogunniyi, *Bioresour. Technol.*, 2006, **97**, 1086–1091.
29 H. Mutlu and M. A. R. Meier, *Eur. J. Lipid Sci. Technol.*, 2010, **112**, 10–30.
30 L. A. Quinchia, M. A. Delgado, J. M. Franco, H. A. Spikes and C. Gallegos, *Ind. Crops Prod.*, 2012, **37**, 383–388.
31 X. Wang, X. Zhai, X. Zou, Z. Li, J. Shi, Z. Yang, Y. Sun, M. Arslan, Z. Chen and J. Xiao, *LWT*, 2022, **164**, 113631.
32 F. Scarpelli, A. Crispini, E. Giorno, F. Marchetti, R. Pettinari, C. Di Nicola, M. P. De Santo, E. Fuoco, R. Berardi, P. Alfano, P. Caputo, D. Policastro, C. Oliviero Rossi and I. Aiello, *ChemPlusChem*, 2020, **85**, 426–440.
33 F. Marchetti, J. Palmucci, C. Pettinari, R. Pettinari, F. Condello, S. Ferraro, M. Marangoni, A. Crispini, S. Scuri, I. Grappasonni, M. Cocchioni, M. Nabissi, M. R. Chierotti and R. Gobetto, *Chem. – Eur. J.*, 2015, **21**, 836–850, and related references .
34 Bruker Analytical X-Ray Systems, SAINT software, Madison, WI, 2003.
35 G. M. Sheldrick, *SADABS Empirical Absorption Program*, 2003.
36 L. Krause, R. Herbst-Irmer, G. M. Sheldrick and D. Stalke, *J. Appl. Crystallogr.*, 2015, **48**, 3–10.
37 G. M. Sheldrick, *Acta Crystallogr., Sect. A: Found. Crystallogr.*, 2008, **64**, 112–122.
38 G. M. Sheldrick, *Acta Crystallogr., Sect. C: Struct. Chem.*, 2015, **71**, 3–8.
39 O. V. Dolomanov, L. J. Bourhis, R. J. Gildea, J. A. K. Howard and H. Puschmann, *J. Appl. Crystallogr.*, 2009, **42**, 339–341.
40 F. Marchetti, C. Pettinari and R. Pettinari, *Coord. Chem. Rev.*, 2005, **249**, 2909–2945.
41 L. A. Quinchia, M. A. Delgado, T. Reddyhoff, C. Gallegos and H. A. Spikes, *Tribol. Int.*, 2014, **69**, 110–117.
42 M. Davidovich-Pinhas, S. Barbut and A. G. Marangoni, *Carbohydr. Polym.*, 2015, **117**, 869–878.
43 ISO-11885: Waters quality – Determination of selected elements by inductively coupled plasma optical emission spectrometry (ICP-OES).
44 EU Food Contact Regulations for Plastics (food packaging and food Regulations 1935/2004, 79/112/EEC and 89/109/EEC) and EU Regulation 10/2011 (The Plastics Regulation) **https://ec.europa.eu/food/food/chemicalsafety/foodcontact/index_eu.htm**.
45 FDA/CFSAN, Food Additives Permitted for Direct Addition to Food for Human Consumption, Silver nitrate-172.167, **https://www.accessdata.fda.gov/scripts/cdrh/cfdocs/cfCFR/CFRSearch.cfm?fr=172.167**.
46 D. Policastro, E. Giorno, F. Scarpelli, N. Godbert, L. Ricciardi, A. Crispini, A. Candreva, F. Marchetti, S. Xhafa, R. De Rose, A. Nucera, R. C. Barberi, M. Castriota, L. De Bartolo and I. Aiello, *Front. Chem.*, 2022, **10**, 884059.
47 L. Benkraled, A. Zennaki, L. Zair, K. Arabeche, A. Berrayah, A. Barrera, Z. Bouberka and U. Maschke, *Polymer*, 2024, **16**, 974.
48 A. Y. Houde, S. S. Kulkarni and M. G. Kulkarni, *J. Membr. Sci.*, 1992, **71**, 117–128.
49 D. K. Pradhan, B. K. Samantaray, R. N. P. Choudhary, N. K. Karan, R. Thomas and R. S. Katiyar, *Ionics*, 2011, **17**, 127–134.
50 D. K. Pradhan, B. K. Samantaray, R. N. P. Choudhary and A. K. Thakur, *Ionics*, 2005, **11**, 95–102.
51 F. Marchetti, J. Palmucci, C. Pettinari, R. Pettinari, M. Marangoni, S. Ferraro, R. Giovannetti, S. Scuri, I. Grappasonni, M. Cocchioni, F. J. Maldonado Hodar and R. Gunnella, *ACS Appl. Mater. Interfaces*, 2016, **8**, 29676–29687.
52 World Health Organization, *Food Safety Fact Sheet*. 2022, **https://www.who.int/news-room/factsheets/detail/food-safety**.
53 H. Gourama, in *Food Safety Engineering. Food Engineering Series*, ed. K. Demirci, A., Feng and H., Krishnamurthy, Springer, 2020, pp. 25–49.
54 R. Gujjarappa, A. K. Kabi, S. Sravani, A. Garg, N. Vodnala, U. Tyagi, D. Kaldhi, R. Velayutham, V. Singh, S. Gupta and C. C. Malakar, 2022, pp. 135–227.
55 M. Larsson, J. Hjärtstam, J. Berndtsson, M. Stading and A. Larsson, *Eur. J. Pharm. Biopharm.*, 2010, **76**, 428–432.